In Situ X-ray Diffraction Studies of the Crystallization of Layered Manganese Thioantimonates(III) under Hydrothermal Conditions

L. Engelke, M. Schaefer, M. Schur, and W. Bensch*

Institut für Anorganische Chemie, Universität Kiel, Olshausenstr. 40, D-24098 Kiel, Germany

Received November 27, 2000. Revised Manuscript Received January 31, 2001

The solvothermal synthesis of the layered compound $Mn_2Sb_2S_5$·DAP (DAP = 1,3-diaminopropane) has been studied using in situ energy-dispersive X-ray diffraction. The results clearly demonstrate that the induction time strongly depends on the reaction temperature. At lower temperatures two crystalline intermediates could be detected. The decay of the second intermediate and the product growth show a strong correlation. A detailed analysis of the extent of reaction α suggests that a small fraction of the intermediate is either dissolved or converted into an amorphous state. The experimentally determined extent of reaction α versus time was compared with various theoretical models. The reaction exponents indicate similar mechanisms for temperatures between 105 and 125 °C. The best agreement is obtained with a first-order reaction and/or phase-boundary-controlled mechanisms. A rigorous analysis reveals that it is highly likely that with increasing α the mechanism changes, suggesting consecutive and/or parallel kinetics as the reaction proceeds. At 130 °C and α > 0.75 a three-dimensional diffusion-controlled process dominates.

Introduction

The number of scientific contributions dealing with the solvothermal synthesis and characterization of new porous materials is still growing and every year about 1000 research papers are published. New materials exhibiting unusual structural architectures and properties are regularly being discovered.[1−5] Many of these materials show unique physicochemical and catalytic properties and in the overwhelming cases oxides are the basis for these materials. The structural diversity and the interesting properties of thio- and selenometalates prepared under solvothermal conditions were recently reviewed by Sheldrick and Wachold.[6]

It must be noted that the processes leading to the formation and crystallization of porous materials under solvothermal conditions are very complex and poorly understood.[7] The mechanistic understanding of the formation of the framework materials is essential for more rational syntheses. Compared to the large number of contributions describing the syntheses and characterization of new framework materials the number of papers devoted to investigations of the mechanisms and/or kinetics of these materials is relatively low. The first study of a zeolite crystallization using in situ energy-dispersive X-ray diffraction (EDXRD) was done in 1992.[8] Since then, different systems were investigated with in situ EDXRD.[9−14]

It was demonstrated in several contributions that the in situ EDXRD using synchrotron radiation is a powerful method for studying kinetics and mechanisms of crystallization processes.[11,13,14] Direct observation offers several advantages over conventional ex situ techniques such as angular-dispersive X-ray diffraction (ADXRD) commonly applied in the laboratories. The in situ approach allows continuous monitoring of the syntheses, and much more data are obtained for one reaction in comparison to ex situ experiments. Most important is that no quenching or further processing of the samples is necessary, thus reducing the risk of alterations that may occur during such manipulations. Therefore, a good reproducibility of the results is achieved as these only depend on the precise reaction conditions. Another important advantage of the in situ technique is the possibility of observing the formation of intermediate phases and their transformation into the final products. Finally, energy-dispersive diffraction allows monitoring at short time scales, for example, minutes instead of hours, using conventional detectors for angular-dispersive X-ray powder diffraction.

Up to now such in situ experiments were mainly restricted to oxidic systems and only one study was

(1) Barrer, R. *Hydrothermal Chemistry of Zeolites*; Academic Press: London, 1982.
(2) Davis, M.; Lobo, R. *Chem. Mater.* **1992**, *4*, 756.
(3) Weller, M.; Dann, S. *Curr. Opin. Solid State Mater. Sci.* **1998**, *3*, 137.
(4) Bensch, W.; Schur, M. *Z. Naturforsch.* **1997**, *52b*, 405.
(5) Schur, M.; Bensch, W. *Z. Anorg. Allg. Chem.* **1998**, *624*, 310.
(6) Sheldrick, W.; Wachhold, M. *Angew. Chem.* **1997**, *109*, 214.
(7) Francis, R.; O'Hare, D. *J. Chem. Soc., Dalton Trans.* **1998**, 3133.
(8) Munn, J.; Barnes, P.; Hausermann, D.; Axon, A.; Klinowski, J. *Phase Transitions* **1992**, *39*, 129.
(9) Evans, J.; Price, S.; Wong, H.; O'Hare, D. *J. Am. Chem. Soc.* **1998**, *120*, 10837.
(10) Francis, R.; O'Brien, S.; Fogg, A.; Halasymani, P.; O'Hare, D.; Loiseau, T.; Férey, G. *J. Am. Chem. Soc.* **1999**, *121*, 1002.
(11) Norby, P.; Hanson, J. *Catal. Today* **1998**, *39*, 301.
(12) Walton, R.; Loiseau, T.; O'Hare, D.; Férey, G. *Chem. Mater.* **1999**, *11*, 320.
(13) O'Brien, S.; Francis, R.; Fogg, A.; O'Hare, D.; Okazaki, N.; Koruda, K. *Chem. Mater.* **1999**, *11*, 1822.
(14) Christensen, A.; Jensen, T.; Norby, P.; Hanson, J. *Chem. Mater.* **1998**, *10*, 1688.

10.1021/cm001234k CCC: $20.00
Published on Web 03/20/2001

performed on a sulfide, that is, on $(NMe_4)_2Sn_3S_7 \cdot xH_2O$ (denoted as TMA-SnS-1).[15]

Recently, we have synthesized and characterized a series of layered thioantimonate(III) compounds with composition $Mn_2Sb_2S_5 \cdot L$ with L = 2·methylamine (MA), 2·ethylamine (EA), 2·propylamine (PA), 1,3-diaminopropane (DAP), and *N*-methyl-1,3-diaminopropane (MDAP).[16,17] Their crystal structures have been described in detail; therefore, only a short description is given here. The primary building units of the topologically identical $Mn_2Sb_2S_5$ frameworks are MnX_6 octahedra (MnS_6 and MnS_4N_2) and trigonal SbS_3 pyramids. Taking into account the commonly observed long Sb−S bonds above 2.8 Å, $Mn_2Sb_2S_4$ hetero-cuban-like assemblies are formed as secondary building units. These in turn are joined into mesh-like layers in the (100) plane (Figure 1a) with pores exhibiting an ellipsoidal shape. The amines are neutral ligands bound to one of the manganese atoms. One-half of the N atoms of the amino ligands is directed into the pores, the other half perpendicular to the layers (Figure 1b). It is emphasized that in contrast to the majority of the frameworks considered here including the layered SnS phases the $Mn_2Sb_2S_5$ network is charge neutral. Thus, the layers are held together basically by weak van der Waals forces of the alkyl groups of the amino ligands. This is a fundamental difference compared to TMA-SnS-1 that is composed of anionic layers and organic ammonium ions between the layers. The formation of this compound has been reported to proceed via a lamellar precursor.[15]

The aim of our in situ EDXRD studies was to explore whether the formation of $Mn_2Sb_2S_5 \cdot$DAP proceeds via a comparable or a different pathway as in the case of TMA-SnS-1. Furthermore, the influence of the reaction temperature was investigated with respect to the kinetics of product growth. These data are essential to understand the fundamental steps of solvothermal syntheses and are a prerequisite for more directional syntheses.

Experimental Section

The title compounds are obtained by reacting elemental Mn (Heraeus 99.9%, 150 mesh), Sb (Heraeus 99.99%, $<80\mu$) and S (Fluka, purum p.a.) in an aqueous solution of the amine (70 vol %). Extensive preliminary investigations of the syntheses performed in the laboratory showed that the compounds form in a wide temperature range from room temperature up to approximately 170 °C. However, at temperatures above 130 °C alkylammonium thioantimonates of composition $A_5Sb_{21}S_{34}$ (A = alkylamines) are observed as byproducts.[17] On the other hand, syntheses at temperatures below 100 °C require several days for completion. The reaction was studied at 105, 110, 120, 125, and 130 °C under isothermal conditions.

For the in situ investigations autoclaves with Teflon liners with an internal diameter of 10 mm and a volume of 7 mL were used. The external diameter was 30 mm and the wall thickness 10 mm to decelerate the heating of the reaction mixture and to accommodate the heating jacket (see below). Independent measurements demonstrated that the delay time until reaction temperature was reached was only about 3 min. At the points where the beam passes the autoclave its thickness was machined down to 0.5 mm.

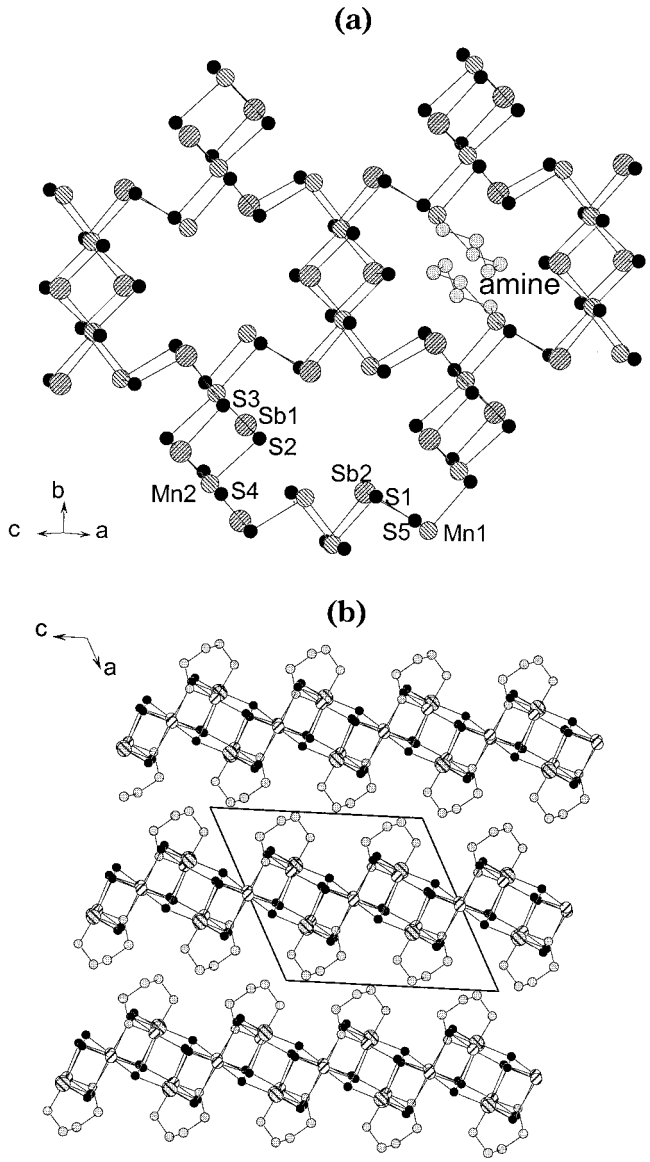

Figure 1. (a) The crystal structure of $Mn_2Sb_2S_5 \cdot$DAP viewed along the (100) plane. (b) Arrangement of the layers of $Mn_2Sb_2S_5 \cdot$DAP.

The in situ measurements were carried out at the HASYLAB-Beamline F3, receiving white synchrotron radiation from a bending magnet with a critical energy of 16.4 keV. The complete reaction cell is shown in Figure 2. The autoclave is fitted with a PARR gage block assembly with a valve and safety rupture disk. Heating was conducted with a self-made heating jacket fitted to the autoclave, consisting of a copper block with appropriate windows for the beam and internal oil circulation connected to a thermostat (JULABO). The temperature was controlled by a thermocouple within the copper block next to the autoclave and regulated to an accuracy of ±1 K. The reactants were intensively mixed by a magnetic stirrer. The whole assembly was adapted to the desk at the beamline. The desk allows both vertical and horizontal adjustment of the cell. The diffracted beam was monitored with a nitrogen-cooled germanium detector. The energy range encloses the range from 13.5 to 65 keV. The number of observable Bragg reflections depends on the detector angle. For our experiments the angle was adjusted at $\Theta = 1.96°$, giving an observable *d* spacing range of 2.8−13.4 Å including the two Sb resonances $K_\alpha = 26.34$ keV and $K_\beta = 29.55$ keV. The most intense (100) reflection of the product is near the intensity maximum.

The amounts of reactants used for the in situ investigation were 0.5 mmol of the solid elements in the stoichiometric ratio

(15) Francis, R.; Price, S.; Evans, J.; O'Brien, S.; O'Hare, D. *Chem. Mater.* **1996**, *8*, 2102.
(16) Bensch, W.; Schur, M. *Eur. J. Solid. State Inorg. Chem.* **1996**, 1149.
(17) Schur, M. Ph.D. Thesis, Frankfurt, 1999.

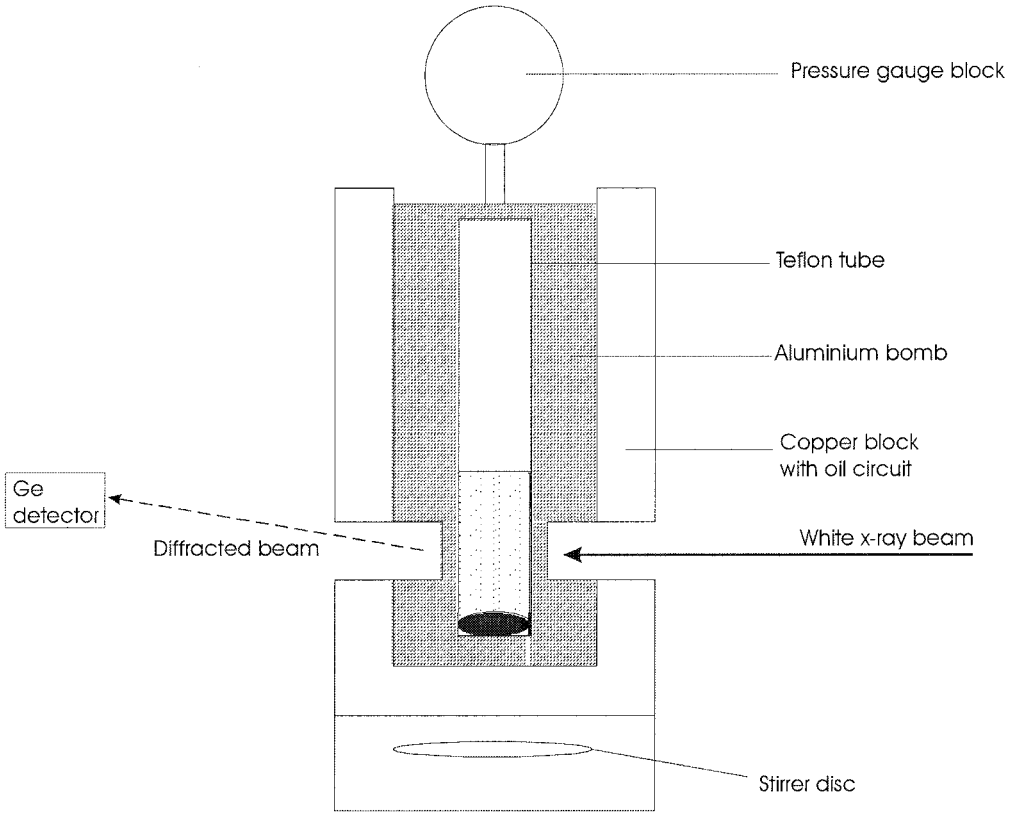

Figure 2. Apparatus used for the in situ experiments.

(27.5 mg of Mn, 61 mg of Sb, 40 mg of S) and 2 mL of amine solution. The delay time between the addition of the amine solution and introduction of the cell into the copper block, which was preheated to the desired reaction temperature in advance, was about 3 min, followed by 1 min until data collection was started. Equilibration of the block-cell assembly to the reaction temperature was <3−4 min, shorter than the induction times observed for the reactions. X-ray diffraction powder patterns were recorded with acquisition times of 300 s. This time period emerged suitable for obtaining sufficient counting statistics and yet short enough for kinetic studies. All spectra were evaluated with the STOE WinXPow and Origin5.0 program packages. The reflection profiles were modeled with a pseudo-Voigt peak shape. To account for the changes of the incident beam power, the intensities of the product reflections were normalized against the peak intensities of the Sb K_α resonance peak.

Results

In the energy range chosen several reflections of the product are monitored simultaneously (Figure 3). A typical result of the time-dependent evolution of the diffraction patterns is shown in Figure 4. The antimony resonances and the (100) reflection of elemental antimony found at $d = 3.11$ Å ($E = 58.3$ keV, not shown in Figure 4) are immediately visible at the beginning of the experiments. After an induction time that strongly depends on temperature product peaks start to grow. The peak with highest intensity is the (100) reflection corresponding to the interlayer spacing of 9.52 Å.

A quantitative analysis of the growth rates demonstrates identical behavior for different reflections at all temperatures investigated. This is depicted in Figure 5 for the most intense (100) and the considerably weaker (−111) reflection recorded at 120 °C and confirms an isotropic crystallite growth.

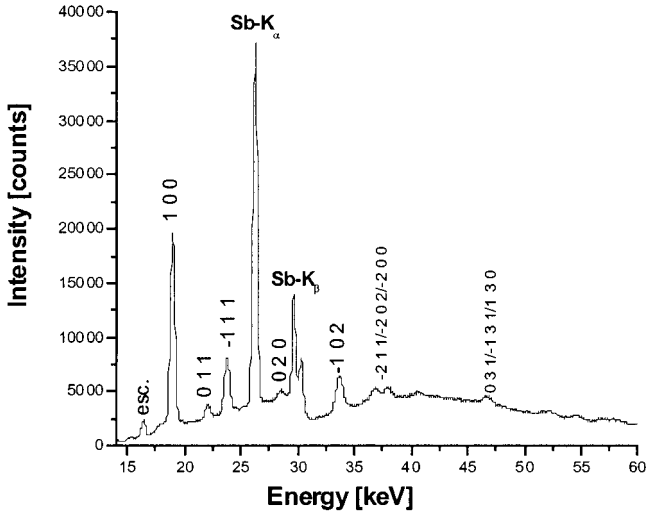

Figure 3. Energy-dispersive diffraction pattern of $Mn_2Sb_2S_5$·DAP. The indices of the reflections and the Sb fluorescence lines are marked. The peak marked with esc. is an escape peak of the Sb fluorescence.

When the temperature was lowered to 105 °C, several additional reflections could be detected, thus indicating the formation of crystalline intermediate phases (Figure 6). During the first 10 min the reflections of a crystalline intermediate with the most intense reflection at $d \cong 6.30$ Å are detected. After several minutes the intensity of the reflections disappeared and reflections of a new phase started to grow with the most intense signal at $d = 9.06$ Å being near the (100) line of the product. The intensity of the lines of this intermediate exhibit no significant alterations until product growth starts. With increasing product formation the intensities of the reflections of the intermediate decreases (Figure 7). We

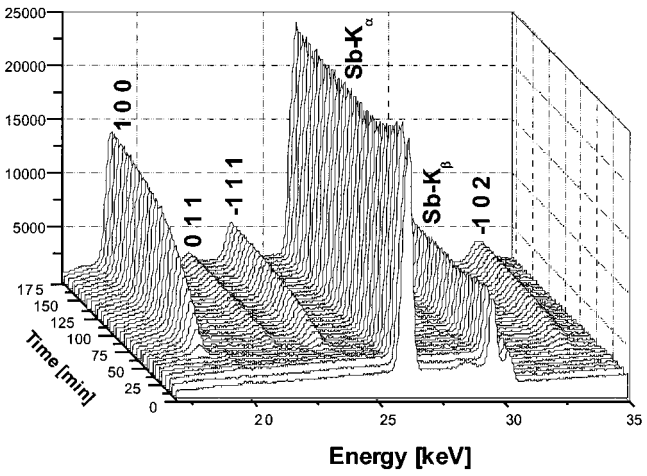

Figure 4. Time-resolved powder pattern recorded at 110 °C. The indices of the most intense lines of the product phase and the Sb fluorescence lines are marked.

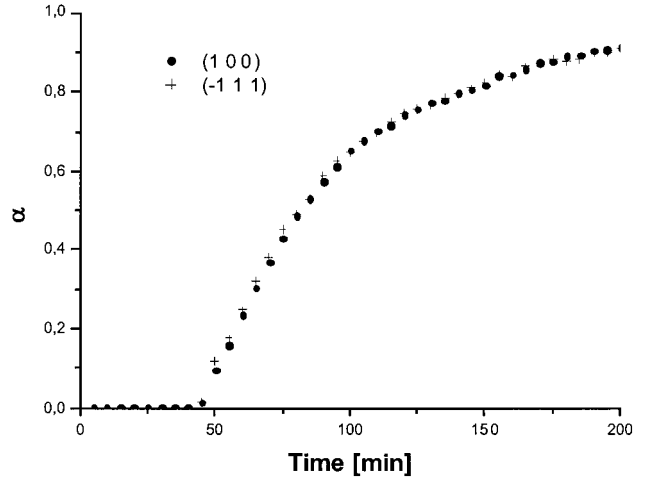

Figure 5. Extent of reaction α versus time for reflections (100) and (−111) at 110 °C.

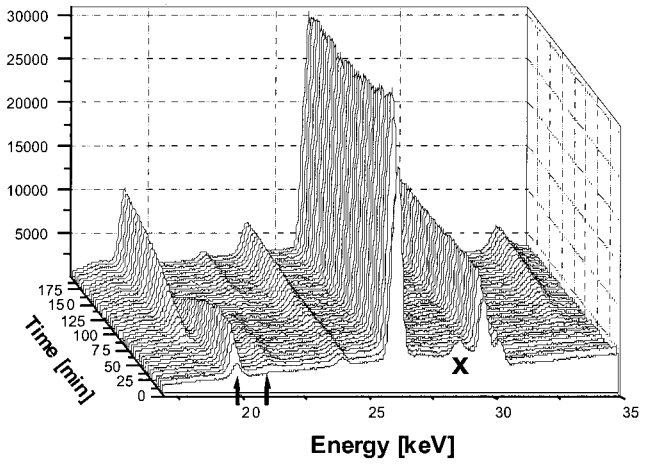

Figure 6. Occurrence of the two crystalline intermediates in the pattern recorded at 105 °C. The marked lines are the most intense lines of the first (cross) and second (arrows) intermediate, respectively.

note that this second intermediate phase could only be detected at temperatures below 105 °C. We cannot exclude that it exists over the whole temperature range. One possibility that the phase is not seen at $T > 105$ °C may be the very short lifetime at elevated temperatures. Additionally, it cannot be ruled out that this

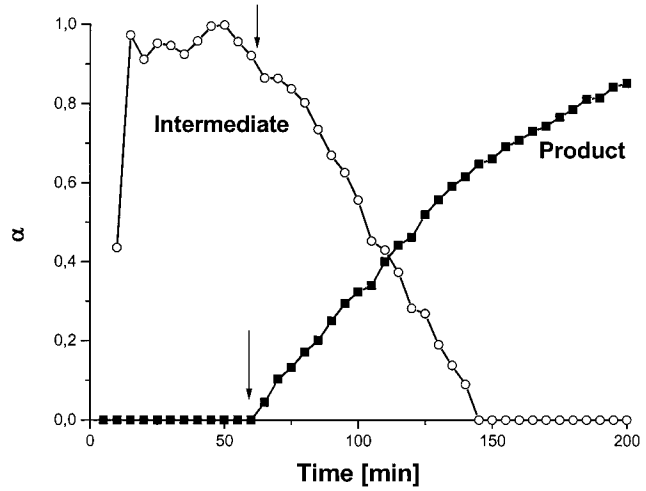

Figure 7. Plot of the extent of reaction α for the second crystalline intermediate and the product extracted from the measurement at 105 °C.

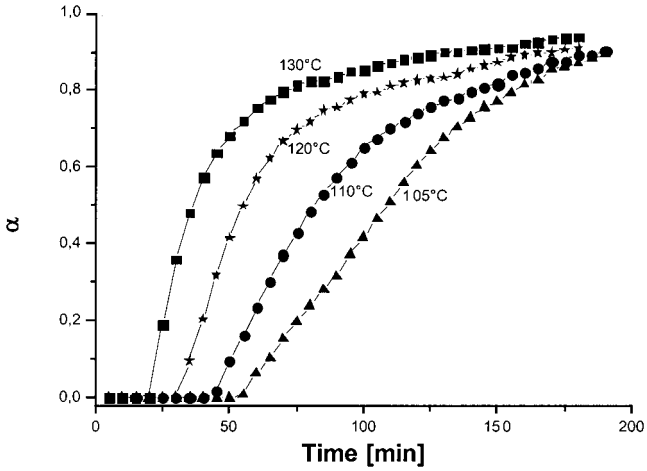

Figure 8. Extent of reaction α versus time for the (100) reflection at different reaction temperatures.

Table 1. Rate Constants *k* and Exponents *m* Obtained by the Analysis with Sharp−Hancock Plots

reaction temperature	t_0 [min]	$t_{0.5}$ [min]	rate constant k [s^{-1}]	exponent (order) m
105 °C	60(5)	124	$2.02(2) \times 10^{-4}$	1.21(2)
110 °C	45(5)	72.5	$2.61(2) \times 10^{-4}$	1.17(1)
120 °C	30(5)	52.5	$3.58(5) \times 10^{-4}$	1.15(4)
125 °C	25(5)	41.5	$4.67(2) \times 10^{-4}$	1.10(1)
130 °C (α < 0.75)	20(5)	32.5	$6.28(2) \times 10^{-4}$	1.02(3)
130 °C (α > 0.75)			$8.47(3) \times 10^{-4}$	0.56(2)

intermediate is not crystalline at higher temperatures. Until now, attempts to trap the two intermediate phases by quenching the reaction mixture and subsequent workup were unsuccessful, indicating that both are decomposed during the cooling procedure or by the following manipulations.

One feature of the crystallization is immediately obvious from Figure 8. The induction time, t_0, which is the time for nucleation, is very short for the highest temperatures applied and increases up to about 60 min at 105 °C (Table 1).

Kinetic Analysis. Kinetic studies are useful because quantitative information such as half-lives and rate constants, about the reactions and the factors influencing them can be obtained. Furthermore, mechanistic information about the reactions studied can be inferred.

Table 2. Functional Forms of Rate Equations Used in Solid State Reactions

growth model[24,26]	rate equation = kt	exponent m
	Diffusion-Controlled	
D1(α)	$\alpha^2 = 0.25(t/t_{0.5})$	0.62
D2(α)	$(1-\alpha)\ln(1-\alpha)+\alpha = 0.1534(t/t_{0.5})$	
D3(α) [Jander]	$[1-(1-\alpha)^{1/3}]^2 = 0.0425(t/t_{0.5})$	0.57
D4(α) [Ginstling−Brounshtein]	$1-2\alpha/3-(1-\alpha)^{2/3} = 0.0367(t/t_{0.5})$	
	Phase-Boundary-Controlled	
R2(α)	$1-(1-\alpha)^{1/2} = 0.2929(t/t_{0.5})$	1.04
R3(α)	$1-(1-\alpha)^{1/3} = 0.2063(t/t_{0.5})$	1.08
	First Order	
F1(α)	$[-\ln(1-\alpha)] = 0.6931(t/t_{0.5})$	1.00
	Nucleation [Avrami−Erovéef]	
A2(α)	$[-\ln(1-\alpha)]^{1/2} = 0.8326(t/t_{0.5})$	2.00
A3(α)	$[-\ln(1-\alpha)]^{1/3} = 0.885(t/t_{0.5})$	3.00

Kinetic analysis is performed by fitting the experimental data to a theoretical expression relating the extent of reaction α and time. Several kinetic expressions applied to solid-state kinetics are reported, and the general shape of their curves is well documented[10,18] (see Table 2).

In the first step of such an analysis the intensity data must be normalized to the theoretical value reached at the end of the reaction ($t = \infty$, $\alpha = 1$). Two steps are necessary to perform the normalization. First, the previously integrated intensities at a time t are divided by the intensity of the Sb K_α resonance peak at the same time to get the normalized intensity relative to the beam intensity:

$$I_n(t) = I_{\mathrm{exp}}/I_{\mathrm{SbK}\alpha}$$

Now the extent of reaction $\alpha(t)$ given as the ratio of the normalized intensity at time t to the intensity at time t_∞ is calculated according to

$$\alpha(t) = I_n(t)/I_n(t_\infty)$$

The kinetic parameters are then obtained by applying the formula

$$\alpha(t) = 1 - \exp[-(kt)^m]$$

with the empirical reaction rate coefficient k and the reaction exponent m. This is the so-called Avrami−Eroféev expression[19−21] that was widely used by several authors.[12,22,23] An evaluation of the normalized intensities can be performed after conversion of the formula to

$$\ln[-\ln(1-\alpha)] = m\cdot\ln(k) + m\cdot\ln(t)$$

When $\ln[-\ln(1-\alpha)]$ versus $\ln(t)$ is plotted, which is the so-called Sharp−Hancock plot,[18] a straight line is obtained for that part of the reaction, which follows the same mechanism. From the slope of the curve the reaction exponent m could be evaluated and the intercept with the y axis gives the rate constant k [s^{-1}]. The kinetic evaluation was performed after subtracting the induction time t_0 from the time t.

In Table 1 the values for the reaction exponent m and the rate constants k are listed for the different reaction temperatures. The data together with the time-resolved growths of the most intense peaks at different reaction temperatures (see Figure 8) emphasize the very fast kinetics of the crystallization and the very short half-life of crystallization $t_{0.5}$ (see Table 1). Increasing the temperature from 105 to 130 °C leads to a significant enhancement of the reaction.

The analysis of the kinetic curves was initially done by fitting the intensity data to the Avrami−Eroféev equation using a least-squares algorithm. Between 105 and 125 °C the exponent m drops from about 1.3 to 1.1. The values obtained were reproducible and for several reactions performed under identical conditions values for m in the range between 1.27(2) and 1.08(2) were obtained. Note that the value of m is very sensitive to the choice of the induction time t_0. At 130 °C the fit was not very good, suggesting that the crystallization does not proceed via one consistent mechanism. The values for the exponents are slightly larger than the values expected for the models F1, R2, or R3 (see Tables 1 and 2).

A more rigorous analysis was performed by testing all models listed in Table 2.[24,25] In addition, the uniformity of the mechanism was examined with a Sharp−Hancock plot as described above. For temperatures up to 125 °C quite good linearity was found, which indicates a consistent mechanism over the whole reaction range (Figure 9). The exponent m ranges from 1.21(2) at 105 °C to 1.10(1) at 125 °C.

At 130 °C the two different regions $\alpha < 0.75$ and $\alpha > 0.75$ can be distinguished. In the first region the exponent m is 1.02(3) and for $\alpha > 0.75$ it drops to 0.56-(2) (Figure 10). This observation suggests that the mechanism changes at higher temperatures, and the low value for the exponent for $\alpha > 0.75$ suggests that the crystallization of the compound under these conditions is a diffusion-controlled process.

On the basis of the above presented results a decision about what model is valid for the crystallization kinetics cannot be drawn. Another way to try to find the correct model is to plot the experimental $t/t_{0.5}$ ($t_{0.5}$ is the reaction time at $\alpha = 0.5$) data versus α, allowing a direct comparison with the different models under consideration.[24] For temperatures up to 125 °C a good agreement

(18) Hancock, J.; Sharp, J. *J. Am. Ceram. Soc.* **1972**, *55*, 74.
(19) Avrami, M. *J. Chem. Phys.* **1939**, *7*, 1103.
(20) Avrami, M. *J. Chem. Phys.* **1940**, *8*, 212.
(21) Avrami, M. *J. Chem. Phys.* **1941**, *9*, 177.
(22) Fogg, A.; O'Hare, D. *Chem. Mater.* **1999**, *11*, 1771.
(23) Thompson, R. *Zeolites* **1992**, *12*, 680.
(24) Sharp, J.; Brindley, G.; Achar, B. *J. Am. Ceram. Soc.* **1966**, *49*, 379.
(25) Hulbert, S. *Br. Ceram. Soc.* **1989**, *6*, 11.

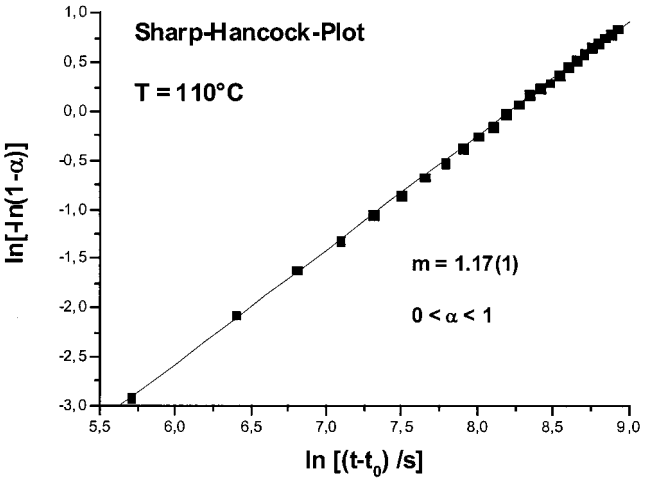

Figure 9. Sharp−Hancock plot for the data obtained at T = 110 °C. For further details, see text.

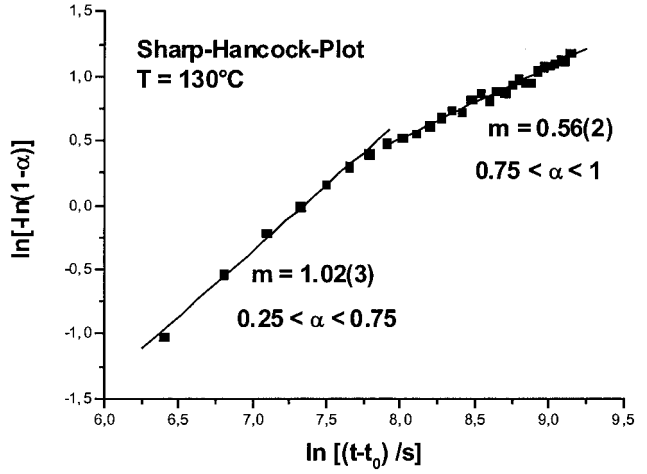

Figure 10. Sharp−Hancock plot for the data obtained at T = 130 °C. For further details, see text.

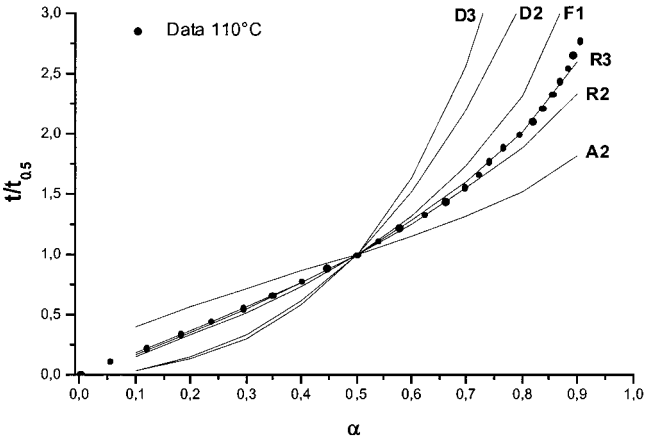

Figure 11. Comparison of the evolution of experimental $t/t_{0.5}$ data as a function of α (black dots) with different theoretical kinetic models for T = 110 °C. The letters with the numbers are the abbreviations of the different models listed in Table 2.

with the models F1, R2, and R3 is obtained (Figure 11). All other models that must be considered can be rejected. It is obvious from Figure 11 that up to α = 0.5 the three models are identical and no distinction is possible. But above α = 0.5 the curves start to diverge moderately and a distinction between the three models

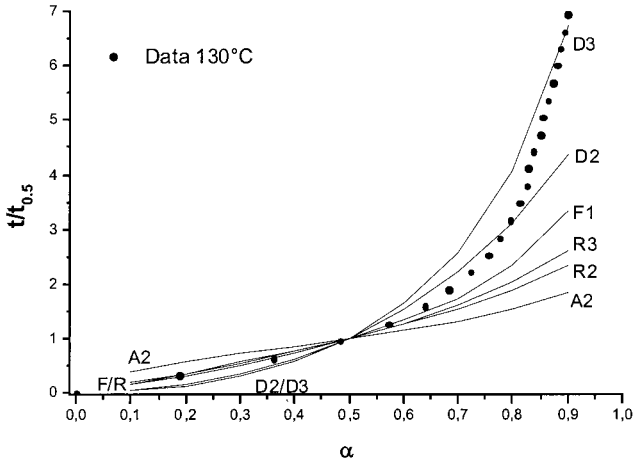

Figure 12. Comparison of the evolution of experimental $t/t_{0.5}$ data as a function of α (black dots) with different theoretical kinetic models for T = 130 °C. The letters with the numbers are the abbreviations of the different models listed in Table 2.

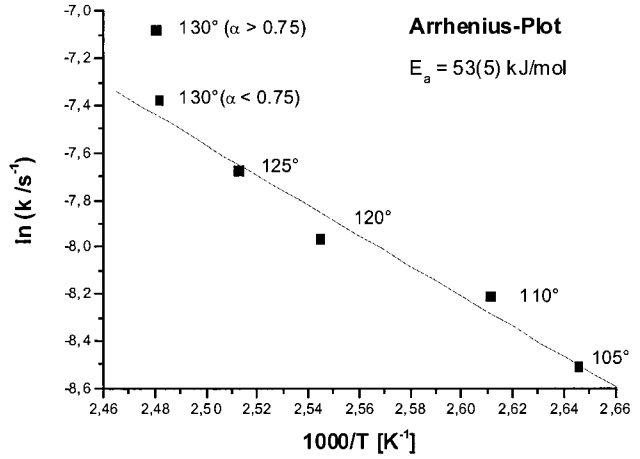

Figure 13. The Arrhenius plot to estimate the activation energy for nucleation. Note that the value ln(k) for T = 130 °C and α > 0.75 is far away from the straight line.

seems to be possible. For the data obtained at T = 110 °C the crystallization kinetics seem to follow model R2 or R3. The situation is different for the data derived at 130 °C. Above about α = 0.65 a significant deviation from the theoretical curves of R2/R3 is seen and at the highest α values the limit of the three-dimensional diffusion-controlled model D3 seems to be reached (Figure 12).

When the values for the rate constant k are inspected, a significant increase with increasing temperature is obtained, and for α < 0.75 at 130 °C it is about 3 times larger than that at 105 °C.

The activation energy of crystallization is calculated with the Arrhenius equation $\ln(k) = \ln(A) - E_a/RT$. As was shown above the mechanism at 130 °C changes at α > 0.75; only the k value obtained for α < 0.75 was taken into account. From the slope of the plot of ln(k) against $1/T$ an activation energy of E_a = 53(5) kJ/mol was obtained (Figure 13).

Discussion

At the beginning of this section it is essential to remember that the first principal steps of the reaction

are multicomponent heterogeneous reactions with different interactions, chemical equilibria, reactions, nucleation, and growth processes. Despite the complexity of hydrothermal crystallization processes the results presented above allow several important conclusions to be drawn.

The temperature strongly influences the so-called induction time t_0 and the velocity of product formation. One should keep in mind that only crystals being larger than a critical size contribute to the observed intensities. Consequently, the measured induction periods represent the time until such large crystallites are formed and give no information about processes such as nucleation. Generally, with increasing temperatures the rate of product growth is enhanced and the kinetics are significantly accelerated.

Between 105 and 130 °C the EDXRD spectra show only reflections of the desired product (together with Sb fluorescence lines) and the reflections of the first intermediate, which disappear after about 10 min. Below 105 °C one additional crystalline phase occurs that starts to grow after several minutes. The intensity of the most intense line of this phase exhibits no significant alterations during the first 30 min and starts to decrease when the first reflections of $Mn_2Sb_2S_5$·DAP occur. The observation of the formation of two crystalline intermediates during the synthesis is clearly of central importance for the understanding of the processes occurring during the formation of the thioantimonate.

With respect to the transformation of the intermediate into the final product, several possibilities must be considered:

(i) Direct solid−solid transformation, no amorphous intermediate, no dissolved phases are involved in the process.

(ii) The intermediate is completely converted into an amorphous phase and the product nucleates and crystallizes subsequently.

(iii) The intermediate is completely dissolved and the product nucleates and crystallizes from the solution.

(iv) Two completely separate processes of the formation of the intermediate and the product occur.

Inspection of Figure 7 gives evidence that the decay of the intensities of the second intermediate phase is highly correlated with the growth of the thioantimonate phase. The onset of the decay occurs simultaneously with the onset of crystallization of the product phase. Therefore, possibility (iv) can be immediately ruled out. Because the curves cross at about $\alpha = 0.4$, it must be assumed that an appreciable amount of the intermediate is either dissolved or converted into an amorphous state. This assumption is further supported by the observation that the reflections of the intermediate disappear before the product reaches $\alpha \approx 1$. The analysis of the fwhm of the most intense reflection of the intermediate reveals no significant change until about 130 min of reaction time and significantly increases above this time. This result suggests that there is no significant loss of crystallinity of the intermediate as the reaction progresses until 130 min, followed by dissolution and/or transformation into the amorphous state. Therefore, it is highly likely that the transformation of the intermediate proceeds via one of the two mechanisms, (ii) or (iii). To fully distinguish between these two possibilities, other in situ measurements are necessary. During the syntheses of aluminophosphates intermediates were detected by in situ NMR experiments.[26,27] But it is obvious that the Mn−Sb−S system is not suitable for such NMR investigations and other techniques such as for instance in situ Raman spectroscopy or in situ XAS may provide the information necessary to understand what happens during the transformation of the intermediate into the final product.

The Sharp−Hancock analysis of the data obtained at different temperatures suggest uniform kinetics of crystallization for temperatures between 105 and 125 °C. At 130 °C the kinetics change at larger α values, and when the temperature is raised above 130 °C, a manganese free product is formed. The reaction exponents m derived for the different temperatures are between about 1.25 (105 °C) and 1.0 (130 °C, $\alpha < 0.75$) with a significantly lower value of 0.56 at 130 °C for $\alpha > 0.75$.

Within the framework of nucleation and growth models the exponent m may be explained with the following model. At lower temperatures and for the first part of reaction at 130 °C the rate of formation of nucleation sites is the most important step and determines the overall rate of crystallization. The rate of growth on the surface of the crystals as well as the transportation rate of the reactive species through the solution to the nucleation sites seem to be less important. With increasing temperature the exponent m decreases, suggesting a successive change of the mechanism with a diffusion-limited mechanism reached at 130 °C for $\alpha > 0.75$. The formation of nucleation sites increases and the reaction produces enough nucleation sites. The rate of reaction for the remaining reaction depends on how fast the material diffuses to the places of crystallization, and the second step is diffusion-limited. The strong increase of the rate constant k with temperature seems to support the conclusions.

The mechanisms discussed must be viewed as ideal borderline cases. One should keep in mind that an interpretation of the exponent m is not straightforward and the discrimination between different mechanisms is not unambiguous and the occurrence of consecutive mechanisms is highly likely. As is obvious from Figure 11 at 110 °C the kinetics follow R2 and/or R3 for $\alpha = 0.5-0.875$ and significantly deviate from the theoretical curves for $\alpha > 0.875$. On the other hand, the data obtained at 130 °C (see Figure 12) start to deviate from the curves of the R2 and R3 mechanisms at $\alpha \approx 0.65$ and seem to follow the curves of the diffusion-controlled mechanisms D2 or D3.

For polycrystalline powders particles of uniform size and shape are required, which is a condition that can seldom be satisfied.[24] But it must be noted that, in most contributions dealing with the kinetics of crystallization, intercalation, and calcination reactions, the analyses were performed on the basis of the Avrami equations and/or Sharp−Hancock plots.[7,9,10,12,14,22,28−32] Therefore,

(26) Koch, E. *Angew. Chem.* **1983**, *95*, 185.
(27) Yu, L.; Pang, W.; Li, L. *J. Solid State Chem.* **1990**, *87*, 241.
(28) Francis, R.; Price, S.; O'Brien, S.; Fogg, A.; O'Hare, D.; Loiseau, T.; Férey, G. *Chem. Commun.* **1997**, 521.

the analysis given above is widely accepted in the scientific community.

It is well-known that the application of the Arrhenius equation to solid-state kinetics is a very crude method and the activation energies extracted contain little physical meaning but are important for the comparison with other systems. Again, we want to note that in many contributions dealing with in situ investigations of the crystallization of porous materials under hydrothermal conditions activation energies of nucleation and crystal growth were derived by applying the Arrhenius equation. According to the discussion presented in ref 12, one should distinguish between the energy for nucleation and the energy for the crystal growth. The former is obtained using the time t_0 and the latter $t_{0.5}$. For the system under investigation E_a amounts to 53(5) kJ/mol using t_0 and is about one-third of the values reported for MnAPO-5 (AFI)[13] or for the synthesis of hydroxysodalite.[33] Keeping in mind that the Si−O/Al−O bond energies are appreciably larger than those of Mn−S/Sb−S, the magnitude of the E_a estimated with the Arrhenius plot seems to be reasonable.

Conclusion

Using in situ EDXRD, we have directly monitored in real time the synthesis of the layered thioantimonate $Mn_2Sb_2S_5$·DAP. The results clearly demonstrate the complexity of solvothermal syntheses and the power of the in situ method. Because of the high time resolution and the quality of the data, kinetic parameters could be extracted and models of the dominating mechanisms of the crystallization could be confirmed. The analyses beyond the so-called Sharp−Hancock plot demonstrate that not only one mechanism is present but also consecutive and/or parallel mechanisms occur as a function of the extent of reaction. The in situ EDXRD experiments at lower temperatures enabled us to identify two different unknown crystalline intermediates/precursors occurring during the synthesis of the thioantimonate. This is an important observation that could not be made by applying the conventional ex situ techniques.

In future projects several efforts are necessary to identify the compositions and structures of the intermediate phases. These compounds may be useful precursors for the syntheses of new thioantimonate compounds. In addition, combined EXAFS/EDXRD experiments are planned to get a better understanding of what happens in solution before crystallization starts. The influence of other parameters such as the nature of the educt, the concentration and kind of the amine, and the grain size of the elements applied are the subject of further studies.

Acknowledgment. We gratefully acknowledge the financial support by the State of Schleswig-Holstein and the Deutsche Forschungsgemeinschaft (DFG). Many thanks also go to Dr. Felix Porsch from HASYLAB.

CM001234K

(29) Davies, A.; Sankar, G.; Catlow, C.; Clark, S. *J. Phys. Chem. B* **1997**, *101*, 10115.
(30) Walton, R.; Smith, R.; Millange, F.; Clark, I.; Sinclair, D.; O'Hare, D. *Chem. Commun.* **2000**, 1267.
(31) Millange, F.; Walton, R.; O'Hare, D. *J. Mater. Chem.* **2000**, *10*, 1713.
(32) Parise, J.; Tan, K.; Norby, P.; Ko, Y.; Cahill, C. *Mater. Res. Soc. Symp.* **1997**, *453*, 103.
(33) Gualtieri, A.; Norby, P.; Artioli, G.; Hanson, J. *Microporous Mater.* **1997**, *9*, 189.